Environmental Engineering and Management Journal

November 2021, Vol. 20, No. 11, 1797-1809
http://www.eemj.icpm.tuiasi.ro/; http://www.eemj.eu

"Gheorghe Asachi" Technical University of Iasi, Romania

NUMERICAL ANALYSIS OF PULSATING FORCED CONVECTION IN A BACKWARD-FACING STEP FLOW SUBJECTED TO NANOFLUIDS

Pınar Sarı Çavdar[1*], Bekir Solmaz[2], Fatih Selimefendigil[3], Ali Yurddaş[3]

[1]İzmir Demokrasi University, Department of Civil Engineering, 35140 İzmir, Turkey
[2]Manisa Celal Bayar University, Department of Civil Engineering, 45140 Manisa, Turkey
[3]Manisa Celal Bayar University, Department of Mechanical Engineering, 45140 Manisa, Turkey

Abstract

The numerical investigation of pulsating forced convection in a backward-facing step flow using water-based nanofluids has been presented. This study is performed for different Reynolds numbers (based on the step height) in the range of 10 and 200, different inlet velocity and different Strouhal number. The effects of water-based nanofluids, which contain Al_2O_3 (Aluminium oxide) and Cu (Copper) nanoparticles with volume fractions ranging from 1% to 5%, on the heat transfer were determined. All numerical solutions were evaluated by using the Finite Volume Method of Computational Fluid Dynamics. The effects of related parameters as Reynolds number and pulsating frequency on the fluid flow and heat transfer characteristics have been numerically analyzed. Increasing the Cu nanoparticle volume ratio gets the heat transfer better than of all.

Key words: backward-facing step flow, forced convection, nanofluids, pulsating flow

Received: November, 2020; Revised final: February, 2021; Accepted: September, 2021; Published in final edited form: November, 2021

1. Introduction

With the increase in the energy costs recently, devices, which provide more effective heat transfer, have started to be designed. One of the ways of heat transfer enhancement is the heat transfer with pulsating flow. Heat transfer with pulsating flow is used in numerous industrial production platforms with military and civilian purposes such as cooling engines and in nuclear reactor cooling systems. In addition, the circulation of blood in the human body is an example of pulsating flow and heat transfer.

Hino et al. (1976) empirically determined the Stokes Boundary Layer thickness regarding the frequency for the shift from laminar flow to the turbulent flow in an oscillatory flow in a tube. Gerrard and Hughes (1971) conducted research on the inlet zone in a system where an oscillatory flow is present. They asserted that the inlet length is much shorter than the steady flow and the typical inlet length equals to the pipe diameter. Thus, the experiments in the study are acknowledged in the full-grown flow zone. Peacock and Stairmand (1983) stated that the inlet velocity profile for the laminar flow does not change since it tends to be flat as in a uniform flow, and the velocity profile is preserved at the inlet and the outlet zones. Atabek and Chang (1961) conducted research on velocity profile at the inlet zone of pulsating flow, and they obtained the velocity distribution analytically. Zamzari et al. (2019) examined the heat transfer effect of a pulsating flow subjected to an external magnetic field along an open space in a horizontal channel.

Different methods have been conducted by many researchers for the enhancement of heat transfer in the systems. In addition to pulsating flow, many factor applications such as magnetic effect, helical wire, steam room for cooling electronic systems, corrugated plate, helically corrugated tube, spirally wound tubes, experimental and numerical study of the

* Author to whom all correspondence should be addressed: e-mail: pinar.cavdar@idu.edu.tr, Phone: +90 232 260 1001, Fax: +90 232 260 1004

micro-fin systems, and the effects of them on heat transfer and pressure were examined detailedly (Naphon, 2016; Naphon and Kornkumjayrit, 2008; Naphon and Sookkasem, 2007; Naphon and Sriromruln, 2006; Naphon and Wiriyasart, 2017, 2018b; Naphon et al., 2013, 2017).

Zhao and Cheng (1998) and Çapkınoğlu and Gündoğdu (2001) showed that surface heat transfer in oscillatory flow changes depending on frequency and amplitude. Gül and Evin (2007) investigated the heat transfer of vibrating pipes. They showed in their study that fluid particles with greater density than the particles near to the pipe walls move faster due to the centrifugal force, and at the same time, the periodical oscillation introduced an extra turbulence to the flow, and thus varying enhancements occur in heat transfer dependent on the frequency and amplitude values.

Selimefendigil and Öztop (2013) performed the numerical analysis of the convection with laminar pulsating flow in an adiabatic thin-edged blade attached to the upper wall of the BFS. They have obtained that the addition of a blade does not have any effect on convective heat transfer of pulsating flow. Khanafer et al. (2008) examined the contributions of laminar flow on mixed convective heat transfer over the BFS. The results have shown that the Richardson number, the Re and non-dimensional wave frequency are effective on the structure of the fluid, heat transfer, and shear stress.

Backward-Facing Step (BFS) flows are the type of flow, which is separated with a reattachment. With the flows separated and reattached behind the step, a turbulence zone is formed, rotating along with the downstream. Accurate calculation of the attachment point of the flow, which is separated and reattached behind the step, has significant importance regarding the flow characteristics, and it is rather an important factor in heat transfer considering that heat transfer reaches its maximum at the reattachment point.

Eaton and Johnston (1981), Vogel and Eaton (1985) studied the heat transfer and flow for the BFS. They also have carried out the research for finding the parameters which change the reattachment length. Eaton and Johnston (1980), Adams et al. (1984) have determined that the Re is an important parameter impacting the flow reattachment length on the BFS. Honami and Nakajo (1986) have performed experimental studies about the effect of the inclined wall on the flow reattachment length, and the effect of the flow expansion length in the BFS, respectively.

Mehrez and Cafsi (2019) numerically investigated the forced convection flow of a hybrid nanofluid over a BFS under a non-uniform magnetic field with the finite volume method. Mehrez et al. (2010) investigated the effects of a periodic perturbation introduced to a separated shear layer behind a BFS by the Large Eddy Simulation (LES) method.

BFS is the most frequently used numerical method since it provides geometrical ease in separated internal flows, Hong et al. (1993), Baek et al. (1993), Abu-Mulaweh et al. (1995), carried out the experimental and numerical study of BFS on laminar, transition and turbulent flows for the range where Re is $70<Re<8000$.

Lin et al. (1990) examined the convective heat transfer of a BFS flow in a complex two-dimensional vertical channel under broad internal flow and wall temperature conditions. Moukalled et al. (2000) studied on the complex convective heat transfer surrounded by an adiabatic wall with varying degrees of incline.

Abu-Nada (2008) developed a model to enhance the heat transfer of flows which includes separated nanofluids and encountered in BFS flow. Williams and Baker (1997), Chiang and Sheu (1999) researched the flow over a 3D BFS. Williams and Baker (1997) investigated the effect of sidewalls in flows, which are three-dimensional and have a Re greater than 400. They studied the complex effect of the main flow of the three-dimensional mechanism and the wall jet. Chiang and Sheu (1999) investigated the effects of laminar flow on account of the decreasing Re in three-dimensional vertical flow over a BFS. Al-Aswadi et al. (2010) examined the effects of nano-particles with a 5% volume of Au, Ag, Al_2O_3, Cu, CuO, diamond, SiO_2 and TiO_2 on forced convection in a two-dimensional BFS. Terhaar et al. (2010) performed experiments of pulsating laminar flow through a two-dimensional BFS. It has been seen that the oscillation effects in heat transfer depend on the geometrical structure.

Various methods are used for enhancing heat transfer efficiency such as oscillation applications, extension of surfaces and microchannel applications. The enhancement of efficiency in heat transfer could be possible with the increase in the conductivity of the fluid used. Usually, fluids that have low thermal conductivity such as water, ethylene glycol and engine oil are used as heat transfer fluids. But thermal conductivity of the base fluid is lower than the solid metals. Solid particles are put in the fluid to increase the thermal conductivity of the base fluid, and it is called the passive enhancement method.

Maxwell (1873, 1904) was the first to come up with the idea that put solid metal particles with a millimeter or micron dimensions in the base fluid. The thermal conductivity of the fluids has been increased by adding solid particles. However, these metal particles, which are heavier than the fluid, caused sedimentation and the microchannels to clog. In addition, they cause erosions and pressure losses. Thus, the idea of adding millimetric or micrometric solid metals did not meet with approval. Wang et al. (2003), Hamilton and Crosser (1962) developed various models for thermal conductivity coefficients using tow-phased mixtures. Due to the applied models, the obtained thermal conductivity coefficients were generally lower than the experimental findings.

Nowadays, nanoparticles that give superior properties to materials and fluids are used in many different areas and applications by Duca et al. (2020), Valipour et al. (2020), Nekoeinia et al. (2020). Wang

and Mujumdar (2007) put forward that nanoparticles added to the base fluid impact the heat transfer and convection properties of the fluid. Xuan and Li (2000) have asserted that the nanoparticles added to the fluid increase the surface area and the thermal capacity of the fluid; they also have pointed out that the effective heat capacity of the fluid is increased. Murshed et al. (2008) indicated that the increment in the thermal conductivity and viscosity of the fluid heavily depend on the volume ratio of the nanoparticles, and there is a direct proportion between temperature and the effective thermal conductivity of the nanofluids. Murshed et al. (2009) advanced a combined model to determine the effective thermal conductivity of the nanofluids. Hwang et al. (2009) studied the convective heat transfer of the Al_2O_3 nanofluid in a fully-grown laminar flow zone. They asserted that an 8% increase is observed in the heat transfer coefficient when the nanoparticle volume ratio was 0.3%. Mansour et al. (2011) investigated the convection of the Al_2O_3-Water nanofluid in a complex inclined pipe under stable heat flux. They expressed a minor decrease in heat transfer by virtue of increment to 4% in nanoparticle volume ratio.

Mehrez and Cafsi (2017) numerically performed the thermodynamic analysis of Al_2O_3-Su nanofluid using the finite volume method in a channel with an open gap under the pulsating inlet state. Naphon et al. (2018) investigated the effects of laminar pulsating flow and nanofluids on heat transfer in a micro-finned tube under a magnetic field. Naphon et al. (2016) performed the experiments of nanofluids with regards to heat transfer and flow properties in horizontal spiral wound tubes. They have argued two correlations for the calculated Nu and friction factor in a spirally wound pipe under constant wall temperature. Naphon et al. (2018) carried out an artificial neural network to examine the heat transfer and pressure drop of pulsating nanofluids in a spirally wound tube under a magnetic field. Naphon and Wiriyasart (2018a) investigated the heat transfer ability of TiO_2-H_2O nanofluid in a helically corrugated tube, taking into account pulsating flow and magnetic field effects.

When the studies in the literature are scrutinized, any study that used the forced convection with pulsating flow over the BFS for nanofluids in the same model is not found. When the studies are investigated, they have shown that using nanofluids provides an enhancement in heat transfer of both flows and oscillated flows over the BFS. Therefore, in this study, the enhancements in heat transfer are obtained by performing forced convection with a pulsating flow over BFSs using different fluids containing different types of nanoparticles with different volume ratios.

2. Case studies

2.1. Defining the model

In this study, the model presented in Fig. 1 is used to perform numerical analysis of forced convection with pulsating flow of a nanofluid over a BFS. The flow of step length of the BFS is H, the height of the channel is 2H. Sinusoidal time dependent velocity is $U = 1 + A\sin(2\pi ft)$, and the uniform temperature is $T_0 = 300K$. In general, numerical investigations of flow over the BFS are used at the inlet parabolic velocity profiles. However, the length of the channel inlet is 10 times greater than the channel height. The downstream length is 35H, from the step to the outlet of the channel. The expression H, which shown in the geometry, equals to 0.1 m. The temperature at the lower surface of the downstream BFS flow is $T_0 = 310K$. Other surfaces are adiabatic, postulating that they do not allow heat transfer. The thermophysical characteristics of the fluid are independent from temperature. The pressure at the outlet of the channel opens to the atmosphere. The flow is postulated as a laminar flow, incompressible and two-dimensional. The natural convection effects are discarded and the forced convection is used in the analysis. Nanofluids are used, obtained by adding Al_2O_3 and Cu nanoparticles in different volume ratio varying between 1% and 5%, into water, the main fluid.

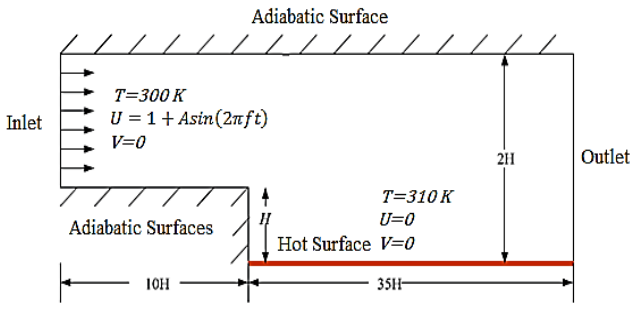

Fig. 1. The schematic presentation of the geometry

In the analyses, water and nanofluids containing nanoparticles such as Al_2O_3 with volume ratios varying between 1% and 5%, and Cu with volume ratios varying between 1% and 2% are used. The channel in our model at the inlet velocity is the sinusoidal and time dependent $U = 1 + A\sin(2\pi ft)$, inlet temperature is 300K, and the temperature at the lower surface of the downstream BFS flow is 310 K. Five different Re values are used (Re= 10, 50, 100, 150, 200). Three different values are used for the A variable in the velocity equation ath the inlet of the channel (A= 0.2; 0.6; 1). Calculations are made for eight different values of the Strouhal Number (St= 0.01; 0.25; 0.05; 0.1; 0.5; 1; 2.5; 5).

Since the sizes of the Al_2O_3 and Cu nanoparticles are too small and they are postulated to distribute homogeneously in water, the fluid is accepted as a mono-phase fluid. Therefore, the mono-phase model is used. In the mono-phase approach, it is accepted that water and the nanoparticles are in thermal balance, and they have the same velocity. Thus, the basic equations of water can also be used for nanofluids. The effects of the nanoparticles are detected by the changes in their thermophysical

characteristics.

Continuous, laminar and incompressible flow conditions are postulated. The relevant system equations under these conditions can be expressed as Eqs. (1-4).

The continuity equation can be expressed by Eq. (1):

$$\frac{\partial u}{\partial x}+\frac{\partial v}{\partial y}=0 \tag{1}$$

X momentum equation (2);

$$\frac{\partial u}{\partial t}+u\frac{\partial u}{\partial x}+v\frac{\partial u}{\partial y}=-\frac{1}{\rho_{nf}}\frac{\partial p}{\partial x}+\nu_{nf}\left(\frac{\partial^2 u}{\partial x^2}+\frac{\partial^2 u}{\partial y^2}\right) \tag{2}$$

Y momentum equation (3);

$$\frac{\partial v}{\partial t}+u\frac{\partial v}{\partial x}+v\frac{\partial v}{\partial y}=-\frac{1}{\rho_{nf}}\frac{\partial p}{\partial y}+\nu_{nf}\left(\frac{\partial^2 v}{\partial x^2}+\frac{\partial^2 v}{\partial y^2}\right) \tag{3}$$

Energy equation (4);

$$\frac{\partial T}{\partial t}+u\frac{\partial T}{\partial x}+v\frac{\partial T}{\partial y}=\alpha_{nf}\left(\frac{\partial^2 T}{\partial x^2}+\frac{\partial^2 T}{\partial y^2}\right) \tag{4}$$

The equations, in which the thermophysical characteristics of the nanofluids to be analysed by postulating that the nanoparticles in the fluid are distributed homogeneously, are represented by Eqs. (5-8).

The expression, in which the density of the nanofluid is defined is given by Eq. (5);

$$\rho_{nf}=(1-\varphi_1-\varphi_2)\rho_f+\varphi_1\rho_{s1}+\varphi_2\rho_{s2} \tag{5}$$

The expression, in which the thermal capacity of the nanofluid is defined is given by Eq. (6);

$$(\rho c_p)_{nf}=(1-\varphi_1-\varphi_2)(\rho c_p)_f+\varphi_1(\rho c_p)_{s1}+\varphi_2(\rho c_p)_{s2} \tag{6}$$

The expression, in which the viscosity of the fluid is defined, as stated by Brinkman (1952) is given by Eq. (7);

$$\mu_{nf}=\frac{\mu_a}{(1-\varphi_1-\varphi_2)^{2,5}} \tag{7}$$

The expression, in which the thermal conductivity of the fluid is defined, as stated by Maxwell (1873) for globular nanoparticles is given by Eq. (5);

$$\frac{k_{nf}}{k_f}=\frac{(k_{s1}+k_{s2})+2k_f-2\varphi_1(k_f-k_{s1})-2\varphi_2(k_f-k_{s2})}{(k_{s1}+k_{s2})+2k_f+\varphi_1(k_f-k_{s1})+\varphi_2(k_f-k_{s2})} \tag{8}$$

The thermophysical characteristics of the nanofluids are determined with the expressions above. Among the terms used above, 'C_p' represents specific heat, 'φ' represents the volume ratio of the nanoparticles in the fluid, '*nf*' subindex represents the nanofluid, '*f*' subindex represents water and the '*s*' subindex represents the nanoparticle.

Table 1 presents the thermophysical characteristics of Alumina, Copper and Water during the analyses in this study. With the equations above, the thermophysical characteristics of the nanofluids are acquired in Table 2. Table 2 shows that the increment in volume ratios of the nanoparticles provides an increment in the viscosity and heat transfer coefficient, but causes a decrease in specific heat and thermal expansion coefficient.

While Al_2O_3 nanoparticles cause an increment in the specific heat and thermal expansion coefficient of the fluid; Cu nanoparticles cause an increment in the density and heat transfer coefficient. The change in viscosity is due to the volume ratio of the nanoparticles in the nanofluid, not to the type of the nanoparticle, by virtue of the equation used.

2.2. Boundary conditions

Boundary conditions are determined as below:

- Inlet velocity at the channel is unidirectional and sinusoidal; temperature and velocity are same in (Eq. 9):

$$U=1+A\sin(2\pi ft),\ V=0,\ T_0=300K \tag{9}$$

- The temperature at the downstream lower surface is constant at the step. $T_0=310\ K$
- The velocity gradient values are 0 for the X direction at the outlet of the channel in (Eq. 10).

Table 1. Thermophysical characteristics of water (20^0c), alumina and copper used in the analyses

	ρ (kg/m^3)	C_p (J/kgK)	k (W/mK)	μ (kg/ms)
Water	997.78	4076.4	0.60475	0.0009772
Al_2O_3	3970	765	40	-
Cu	8933	385	401	-

Table 2. Thermophysical characteristics of the nanofluids with regard to the volume ratio of nanofluids used

φ(%) Al_2O_3+Cu	ρ (kg/m^3)	C_p (J/kgK)	k (W/mK)	μ (kg/ms)
% 1 + % 1	1106.8544	3659.7098355	0.6229743	0.0010278
% 3 + % 1	1166.2988	3455.5123664	0.6262855	0.0010822
% 5 + % 1	1225.7432	3271.12067069	0.6296088	0.0011407
% 3 + % 2	1245.651	3230.341783	0.6432563	0.0011109

$$\frac{\partial U}{\partial X} = O\,,\ \frac{\partial V}{\partial X} = O\,,\ \frac{\partial T}{\partial X} = O \qquad (10)$$

No-slip conditions at the channel walls (except for the downstream step) and at the adiabatic walls $U = 0$, $V = 0$, $\frac{\partial \vartheta}{\partial n} = O$; n represents the normal surface.

2.3. Mesh analysis

One of the important steps for a study with numerical analyses to be sound is to perform the mesh analysis accurately. Increasing the number of the mesh does not mean that the analysis would yield results that are more accurate. Performing the analysis with greater number of mesh than required would increase the time required for the solution, although it would yield an accurate result. Therefore, the network analysis presented in Table 3 is conducted by comparison of the Average Nu values that correspond to the number of the nodes and the number of the elements.

Table 3. Mesh analysis (Selimefendigil and Öztop, 2013)

	Cell Number	***Nusselt Number***
G1	3968	1.0369
G2	8928	1.0353
G3	15 872	1.0347
G4	24 800	1.0345

In the network analysis for the Reynold number 100 in Table 1, the geometry is separated into 15872 triangular elements, and when the *Nu* is considered, it is seen that the optimal structure is the G3 structure. All analyses are performed with this network structure in order to make the comparisons more accurately.

2.4. Verification of the study

The numerical code is first verified by the flow over a BFS in the literature. In Table 4, the values obtained by the division of the downstream length for Re 100 to the height of the step are compared. The lowest error rate is -2.93% and the highest error rate is -6.83%. As the general error rate is smaller than 5%, the numerical code is used. The verification analyses for numerical code with the codes in the literature and the error rates pertaining to these are presented in Table 4.

The equations are performed via the ANSYS FLUENT software package which uses the finite volumes method. In the momentum equations, the SIMPLE solution algorithm with the finite volume's method has been applied to evaluate the pressure-velocity couple. The convergence value in the continuity equation is accepted as 10^{-3}, the convergence value in the momentum equations is accepted as 10^{-5}, and the convergence value in the Energy equation is accepted as 10^{-6}.

Table 4. Values obtained by the division of the downstream length for Reynolds number 100 to the height of the step (Selimefendigil and Öztop, 2013)

	X_R/S	***Error (%)***
Acharya et al. (1993)	*4.97*	*-2.93*
Lin et al. (1990)	4.91	-4.1
Dyne et al. (1993)	4.89	-4.49
El-Refaee et al. (1996)	4.77	-6.83
Cochran et al. (1993)	5.32	3.9
This Study	5.12	0

3. Results and discussion

3.1. Continuous regime

In Fig. 2, the velocity distributions in different Reynold numbers are presented using nanofluids comprising of water and various volume ratios (1-5%) of Al_2O_3 and various volume ratios (1% or 2%) of Cu nanoparticles. The colour change in the spectrum represents the change in velocity. While red is representing the highest velocity, blue represents the lowest velocity. The velocity distributions for water fluid without any nanoparticles are presented in Figs. 2a-e plotted by using the Reynolds numbers 10, 50, 100, 150 and 200 (Re) respectively. As the Re increases, the cycle from step to reattachment also increases.

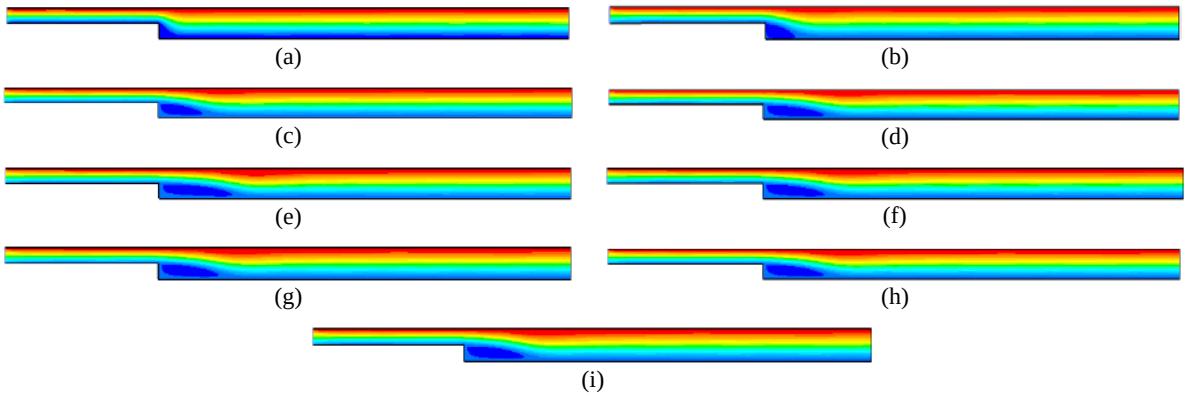

Fig. 2. The velocity distributions for (a) ϕ_1=0, ϕ_2=0 Re=10; (b) ϕ_1=0, ϕ_2=0 Re=50; (c) ϕ1=0, ϕ2=0 ve Re=100; (d) ϕ1=0, ϕ2=0 Re=150; (e) ϕ_1=0, ϕ_2=0 Re=200; (f) ϕ_1=0.01, ϕ_2=0.01 Re=150; (g) ϕ_1=0.03, ϕ_2=0.01 Re=150; (h) ϕ_1=0.05, ϕ_2=0.01 Re=150; (i) ϕ_1=0.03, ϕ_2=0.02 Re=150

Fig. 3 present the temperature changes in different Re using the nanofluids comprising of water and various volume ratios of various volume ratios (1-5%) of Al_2O_3 and various volume ratios (1% or 2%) of Cu nanoparticles. Blue represents the lowest temperature (300 K), and red represent the highest temperature (310 K). The temperature from the step towards the downstream decreases as the Reynold number increases.

Fig. 4 compares the change of Nu through the hot surface for different Reynolds numbers. Figure show that the heat transfer capability has been increased in the main fluid and in other nanofluids by virtue of an increment in Re. Some cases are observed in which the Nu peaked, as the heat convection coefficient increases too much when compared to the heat transfer coefficient. After these increase zones, the Nu comes to a balance. This transition to balance condition increases with increment in Re because as the Re increases, the number of the peaks increase.

Fig. 5 presents the change of the ratio of average Nu of water and nanofluids containing various volume ratio of different nanoparticles to the initial Nu, with reference to the Re. It is seen that the heat transfer capabilities of nanofluids are better than water. As for the nanofluids, it is seen that their heat transfer capabilities increase as their nanoparticle volume ratio increases. As the volume ratios of the Al_2O_3 nanoparticles in the nanofluids increase, any significant change could not be observed in heat transfer; however, a significant increase in the heat transfer capability of the nanofluid is observed as the volume ratio of Cu nanoparticle increases.

Fig. 6 investigates the change of the friction coefficient in continuous flow condition throughout the hot surface for different nanofluids. It shows that the friction coefficient decreases with an increment in Re. Since the velocity increases with increment in Re, the friction coefficient decreases inversely proportionally.

The change in the volume ratio or type of the nanoparticle does not change the friction coefficient. As forced convection is postulates in the analyses, the effects of natural convection are discarded. Therefore, the change in fluid type does not have an impact on the friction coefficient.

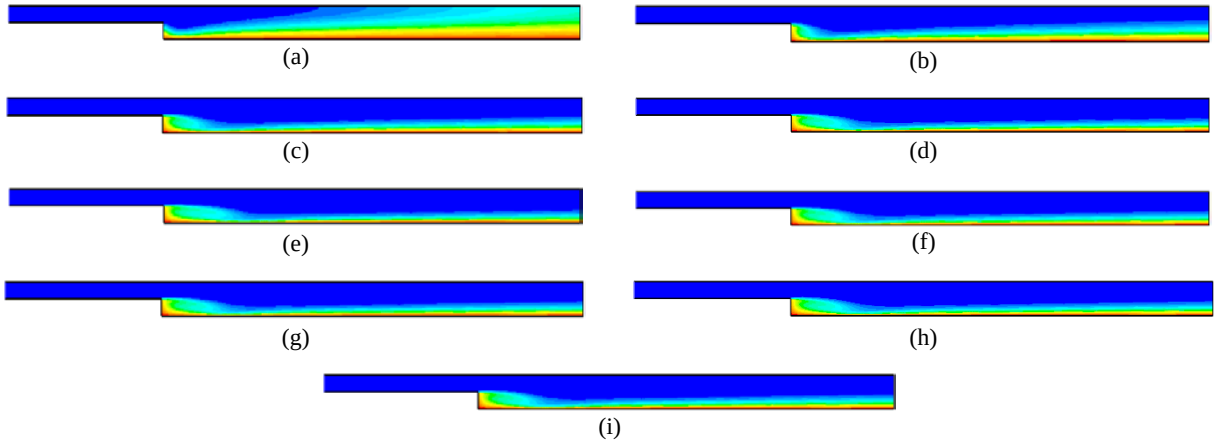

Fig. 3. The temperature changes in (a) ϕ1=0, ϕ2=0 ve Re=10; (b) ϕ1=0, ϕ2=0 ve Re=50; (c) ϕ1=0, ϕ2=0 ve Re=100; (d) ϕ1=0, ϕ2=0 ve Re=150; (e) ϕ1=0, ϕ2=0 ve Re=200; (f) ϕ1=0.01, ϕ2=0.01 ve Re=150; (g) ϕ1=0.03, ϕ2=0.01 ve Re=150; (h) ϕ1=0.05, ϕ2=0.01 ve Re=150; (i) ϕ1=0.03, ϕ2=0.02 ve Re=150

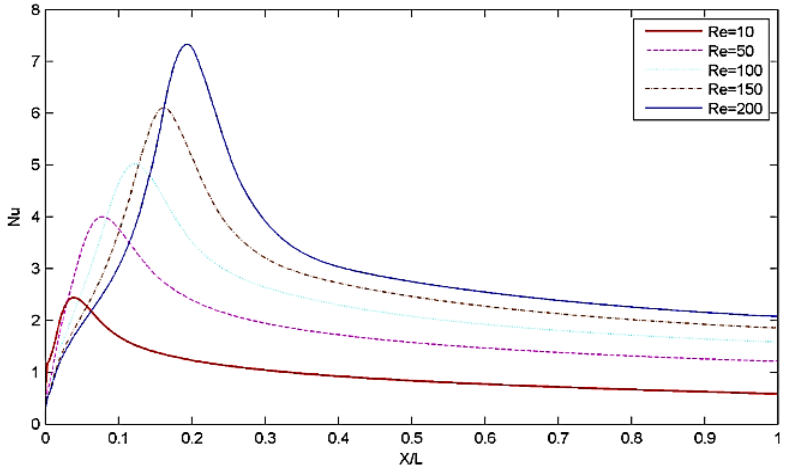

Fig. 4. The change of Nusselt number throught the hot surface for different Reynolds numbers (ϕ_1= ϕ_2=0)

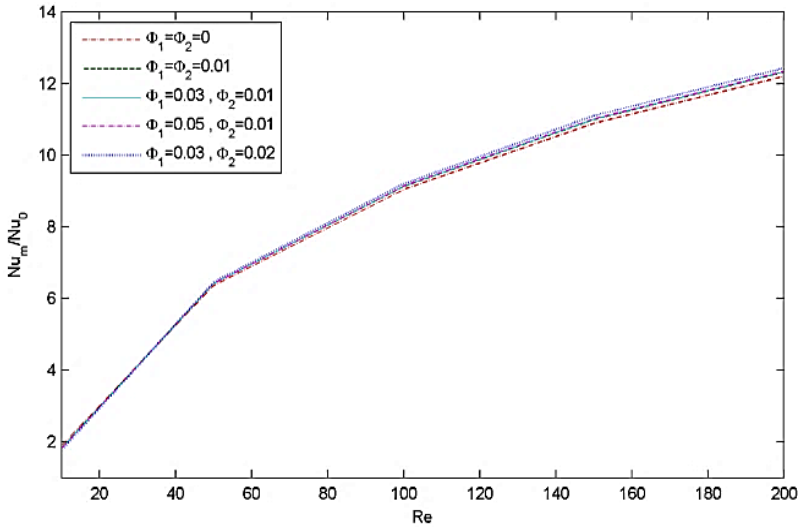

Fig. 5. The change of the ratio of average Nusselt number of nanofluids containing various volume ratio of different nanoparticles to the initial Nusselt number, with reference to the Reynolds number

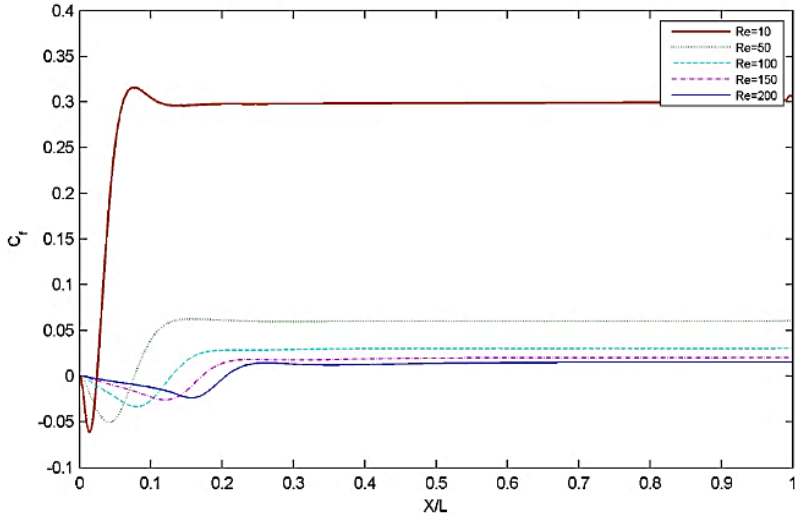

Fig. 6. The change of the friction coefficient in continuous flow condition throughout the hot surface for different nanofluids. ($\phi_1 = \phi_2 = 0$)

3.2. Pulsating flow

Fig. 7 shows how Re change Nu under an pulsating flow condition, in which the velocity amplitude is 0.6, and Strouhal number is 0.5. As it can be seen in the figure, the increase in Re increases the heat transfer capability in water, the main fluid, and in other nanofluids. The reason for the amplitudes are not clear in the figure is that the increase in Reynolds numbers cause extreme changes in the Nu.

Fig. 8 makes a comparison of different velocity amplitudes (A=0.2, A=0.6, A=1) on the Nu and time graphics. It is seen that the increase in the velocity amplitudes of water and nanofluids causes significant increases in the Nu. It is understood from these figures that velocity amplitude value in pulsating flow has a great significance in heat transfer capability. The Re is accepted as 100 and the Strouhal number as 0.5, in order to make a sounder comparison of these figures.

The analyses are conducted for different Strouhal numbers (St=0.01, St=0.05, St=0.1, St=0.25, St=0.5, St=0.1, St=2.5, St=5). Fig. 9 shows the change of the average Nu with regard to the Strouhal number. The impact of the different Reynolds numbers on these figures are also determined. The increase in the Re causes a significant increase in the Nu in all fluids. The average Nu comes to a balance as the Strouhal number increases, after making a peak in some zone of small values of Strouhal number. This is caused by the effect of lower frequency values on the change of velocity over time in momentum equations. This peak condition increases as the Re increases.

The effect of different velocity amplitudes on the average Nu is presented in Fig. 10. It is seen that the average Nu increases as the velocity amplitude increases. As it can be seen in the Figures, pulsating flow significantly increases the heat transfer capability of a fluid. This increase is present in water and other nanofluids.

The enhancement in the heat transfer capability introduced by the pulsating flow induced by increasing the velocity amplitude is more favourable than the enhancement by using different fluid (nanofluid) at a constant velocity amplitude.

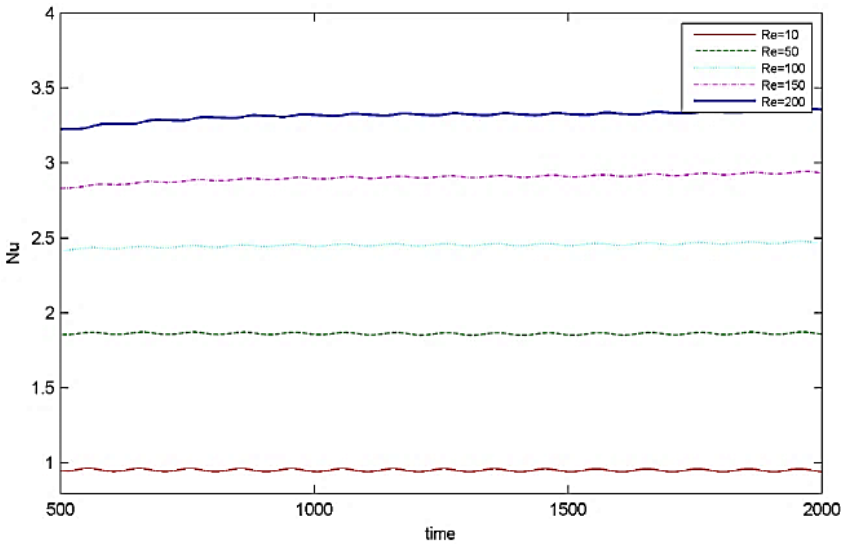

Fig. 7. The Nusselt Number Change with time in Different Reynolds number change (ϕ_1=ϕ_2=0.01, A=0.6, St=0.5)

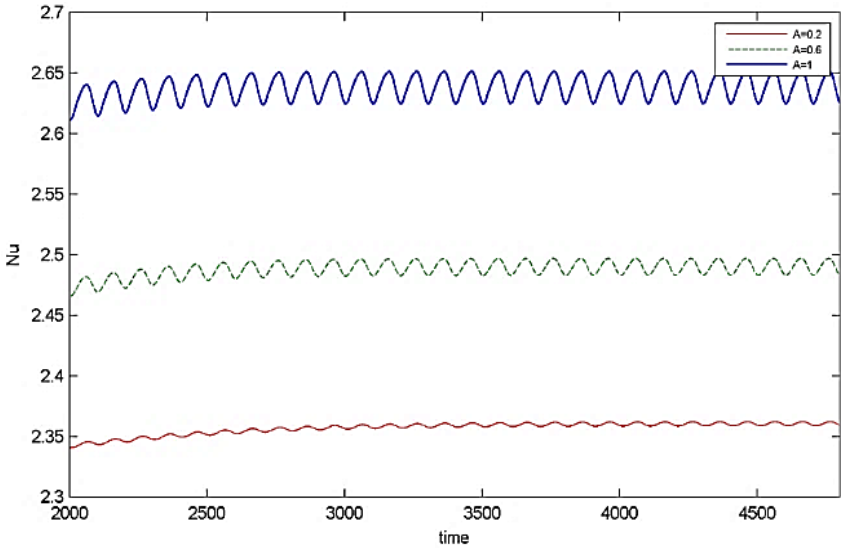

Fig. 8. The Nusselt Number Change with time in Different velocity amplitude change (ϕ_1=0.01, ϕ_2=0.01, Re=100, St=0.5)

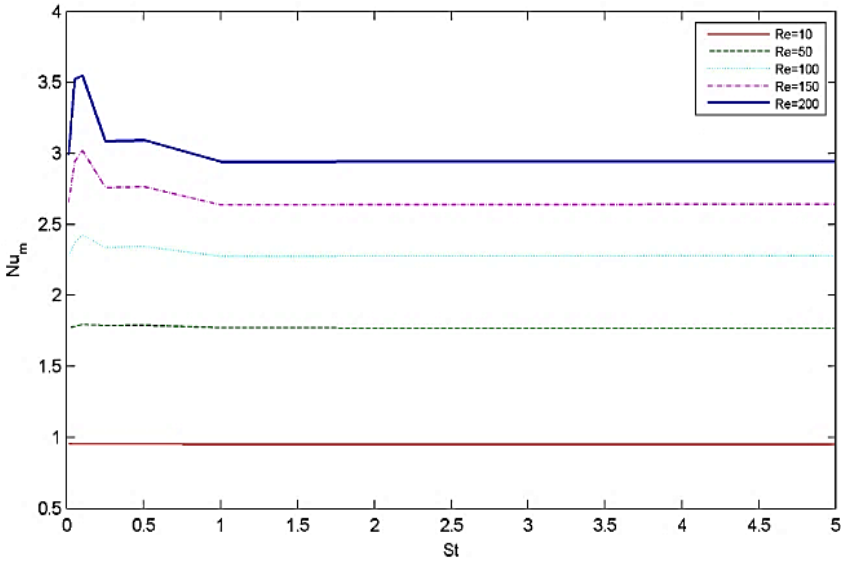

Fig. 9. The Change of Nusselt Number in different Reynolds number according to Strouhal Values (ϕ_1=ϕ_2=0.01, A=0.2)

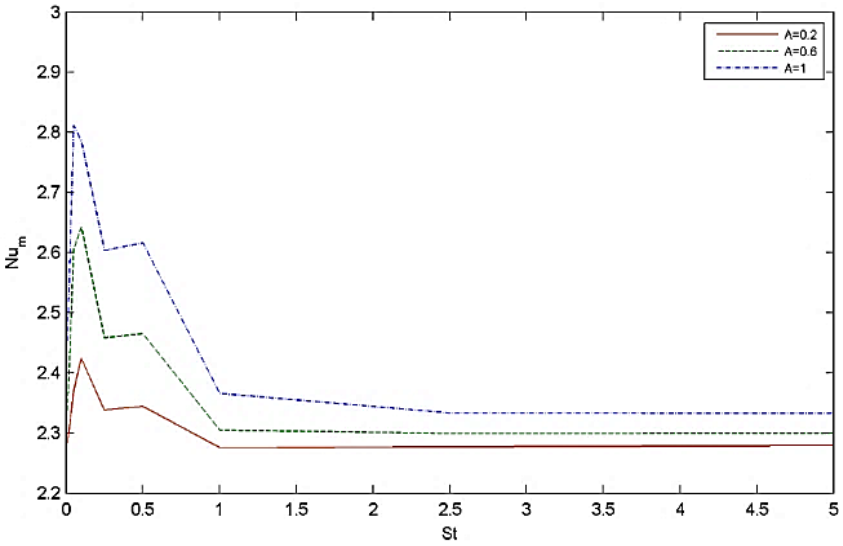

Fig. 10. The Change of Nusselt Number in different velocity amplitude according to Strouhal Values (ϕ_1=ϕ_2=0.01, Re=100)

Fig. 11 compares the change in friction coefficient in pulsating flow condition for different Reynolds numbers. In pulsating flow condition, the increase in the Re causes a decrease in the friction coefficient. The friction coefficient of a nanofluid containing 1% volume ratio of Al_2O_3 and 1% volume ratio of Cu nanoparticles is slightly lower when compared to other fluid types. The friction coefficients of other fluids are almost the same. This is caused by the shear stress of the fluids.

Fig. 12 examines the change in the friction coefficient for different velocity amplitudes under pulsating flow condition. The friction coefficient decreases as the velocity amplitude increases, as expected. For the nanofluids other than the nanofluid containing 1% volume ratio of Al_2O_3 and 1% volume ratio of Cu nanoparticles, and the main fluid, water, the friction coefficient is almost the same. The friction coefficient for the nanofluid containing 1% volume ratio of Al_2O_3 and 1% volume ratio of Cu nanoparticles is slightly lower when compare to other fluid types. This is caused by the shear stress of the nanofluid.

Fig. 13 shows what kind of a change the difference in the Strouhal number would cause in the friction coefficient. It is seen that the friction coefficient increases as the Strouhal number increases. This situation is caused by the increase in frequency values directly proportional to the increase in the Strouhal number.

Fig. 14 investigates the effect of change in fluid type, the change of velocity amplitude, and the change of frequency on the flow conditions in the model, when the flow is pulsating. As expected, the increase in the Re increases the velocity and thus increases the circulation before the step. In smaller Reynolds numbers, it is seen that the flow lines between the boundaries are irregular, and these become more regular as the Re increases. In addition, the hydrodynamic behaviour of the fluid in pulsating flow resembles to the behaviour in continuous flow, as the Re increases. In smaller Re, on the other hand, in pulsating flow conditions, the fluid flows faster in zones closer to the hot surface, when compared to continuous flow conditions. The circulation before the step increases as the volume ratio of Al_2O_3 nanoparticle increases. The circulation before the step disappears as the volume ratio of Cu nanoparticle increases, and the velocity reduces in the zone where the step and hot surface combine. In addition, the velocity throughout the hot surface decreases as the ratio of Cu increases. The velocity of the fluid in this zone decreases since the density of copper is higher than the density of Alumina. When these graphics are compared with the graphics for the continuous regime for the same values, it is seen that the nanofluid containing 1% of Al_2O_3 and 1% of Cu nanoparticles, and the nanofluid containing 3% Al_2O_3 and 1% of Cu nanoparticles present a better hydrodynamic behaviour in pulsating flow when compared to continuous flow. It is seen that the velocity of the fluid increases as the velocity amplitude value increases. The optimal hydrodynamic behaviours of the fluids are observed at the frequency level when the Strouhal number is 0.25.

Fig. 15 investigates the effect of change in fluid type, the change of velocity amplitude, and the change of frequency on the temperature distribution in the model under pulsating flow condition. While the Re is increasing, the heat transfer increases as directly proportional. When it is compared with the continuous flow using the same values, it is determined that the increase in heat transfer is higher in pulsating flow condition.

The change of fluid type in pulsating flow condition causes an insensible, small increase in heat transfer. When continuous flow and pulsating flow are compared, it is seen that different fluid types cause more significant changes in heat transfer, under pulsating flow condition. The increment in velocity amplitude enhances the heat transfer. The change in heat transfer occurs depending on the Strouhal number. However, this change is fixes after a certain Strouhal value.

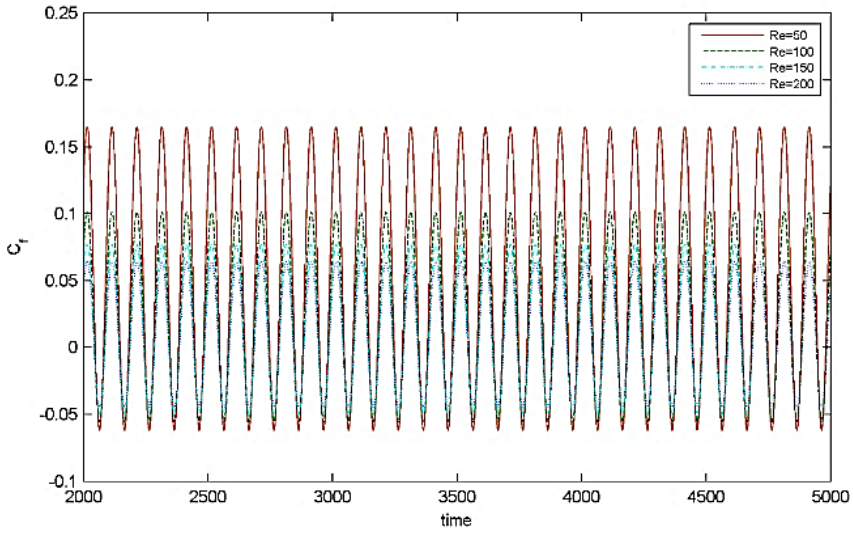

Fig. 11. The Change of Friction coefficient in the different Reynolds number, according to time (ϕ_1= ϕ_2=0.01, A=0.6, St=0.5)

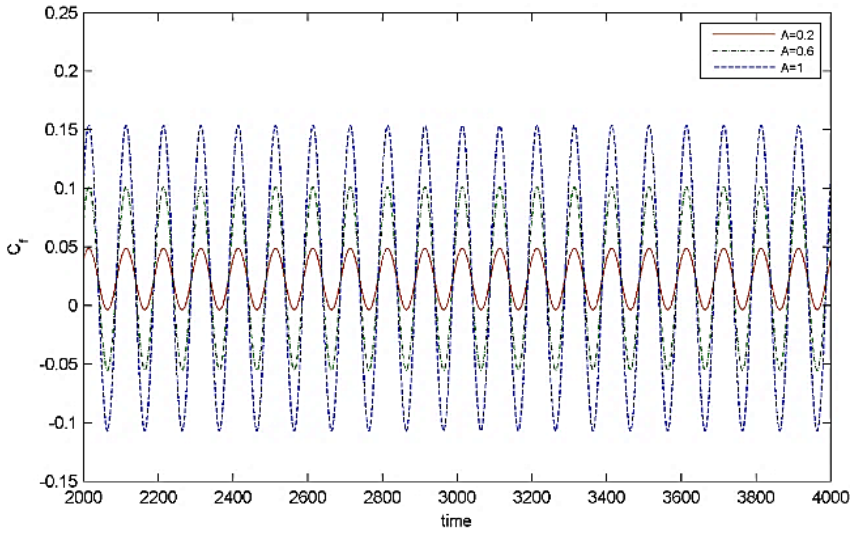

Fig. 12. The change in the friction coefficient for different velocity amplitudes under pulsating flow condition (ϕ_1=ϕ_2=0.01, Re=100, St=0.5)

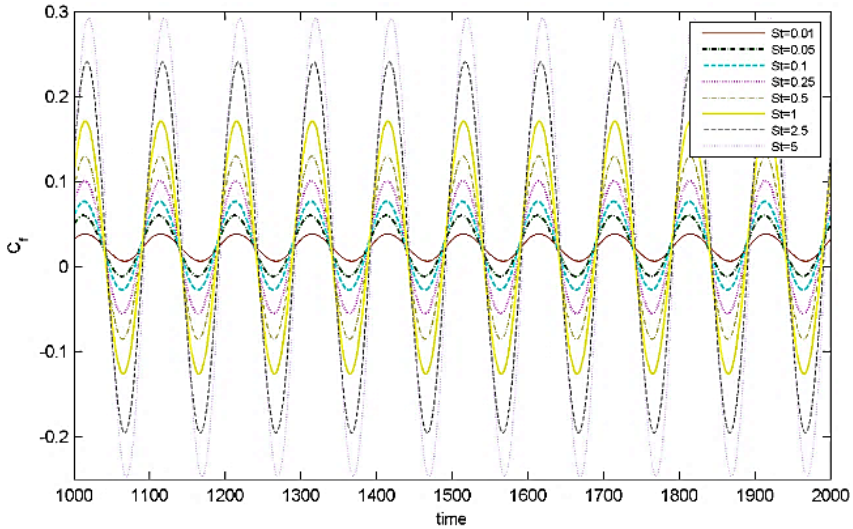

Fig. 13. The change Friction coefficient in the different Strouhal number (ϕ_1=0.03, ϕ_2=0.01, Re=100, A=0.6)

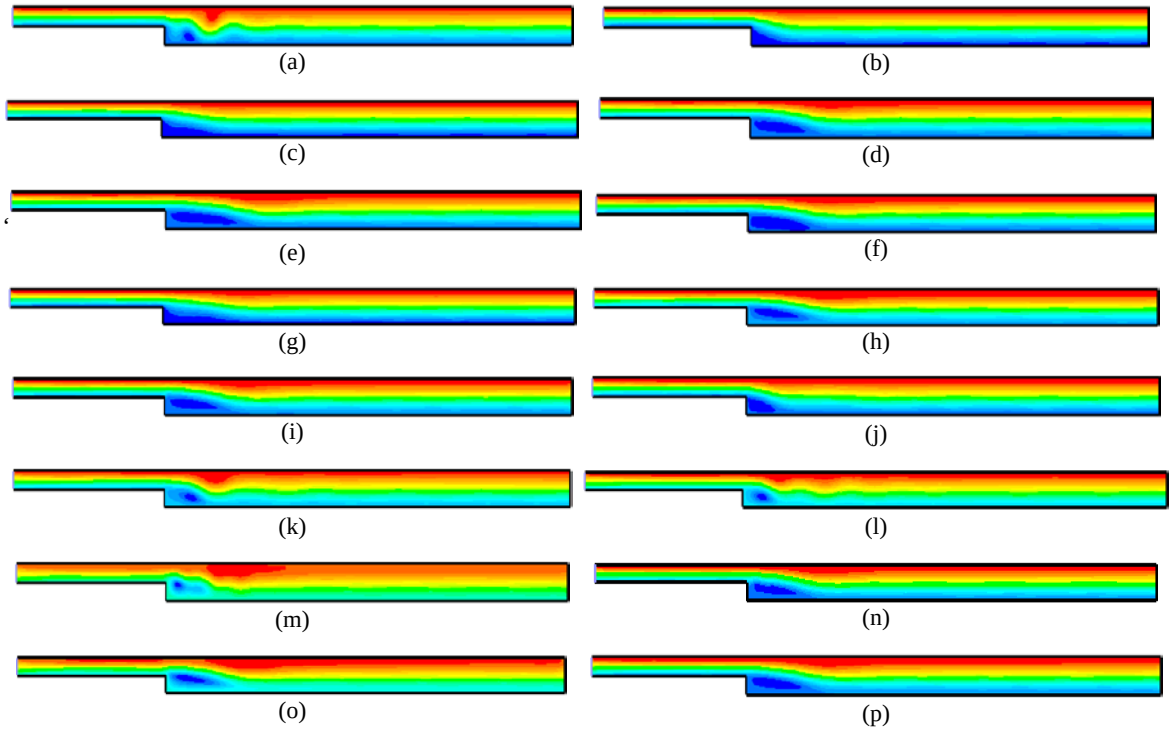

Fig. 14. The velocity distributions of water when the pulsating flow (a) ($\phi1$=0, $\phi2$=0, Re=10, A=0.6, St=1),(b) ($\phi1$=0, $\phi2$=0, Re=50, A=0.6, St=1), (c) ($\phi1$=0, $\phi2$=0, Re=100, A=0.6, St=1), (d) ($\phi1$=0, $\phi2$=0, Re=150, A=0.6, St=1), (e) ($\phi1$=0, $\phi2$=0, Re=200, A=0.6, St=1), (f) ($\phi1$=5, $\phi2$=1, Re=150, A=0.6, St=1), (g) ($\phi1$=3, $\phi2$=2, Re=150, A=0.6, St=1), (h) ($\phi1$=3, $\phi2$=1, Re=150, A=0.2, St=1), (i) ($\phi1$=3, $\phi2$=1, Re=150, A=1, St=1), (j) ($\phi1$=3, $\phi2$=1, Re=150, A=0.6, St=0.01), (k) ($\phi1$=3, $\phi2$=1, Re=150, A=0.6, St=0.05), (l) ($\phi1$=3, $\phi2$=1, Re=150, A=0.6, St=0.1), (m) ($\phi1$=3, $\phi2$=1, Re=150, A=0.6, St=0.25), (n) ($\phi1$=3, $\phi2$=1, Re=150, A=0.6, St=0.5), (o) ($\phi1$=3, $\phi2$=1, Re=150, A=0.6, St=2.5), (p) ($\phi1$=3, $\phi2$=1, Re=150, A=0.6, St=5)

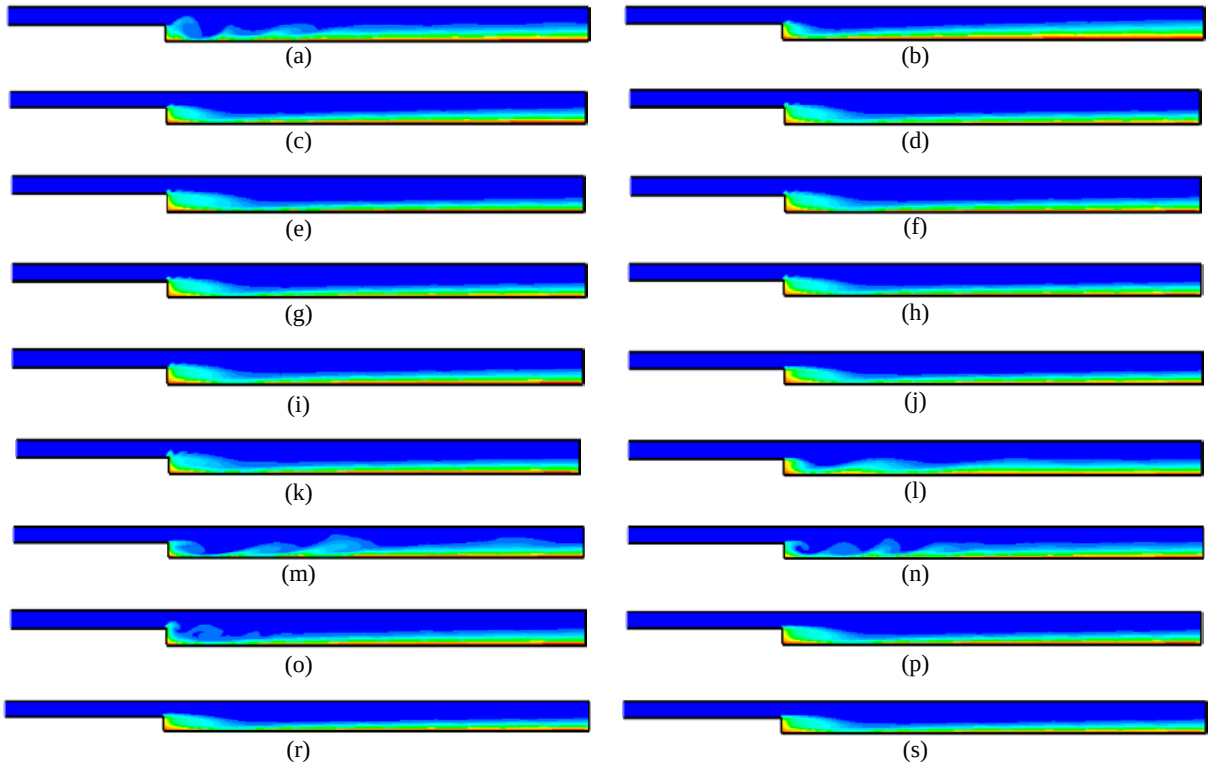

Fig. 15. The temperature distributions of water when the pulsating flow (a) (ϕ_1=0, ϕ_2=0, Re=10, A=0.6, St=1), (b) (ϕ_1=0, ϕ_2=0, Re=50, A=0.6, St=1), (c) (ϕ_1=0, ϕ_2=0, Re=100, A=0.6, St=1), (d) (ϕ_1=0, ϕ_2=0, Re=150, A=0.6, St=1), (e) (ϕ_1=0, ϕ_2=0, Re=200, A=0.6, St=1), (f) (ϕ_1=1, ϕ_2=1, Re=150, A=0.6, St=1), (g) (ϕ_1=3, ϕ_2=1, Re=150, A=0.6, St=1), (h) (ϕ_1=5, ϕ_2=1, Re=150, A=0.6, St=1), (i) (ϕ_1=3, ϕ_2=2, Re=150, A=0.6, St=1), (j) (ϕ_1=3, ϕ_2=1, Re=150, A=0.2, St=1), (k) (ϕ_1=3, ϕ_2=1, Re=150, A=1, St=1), (l) (ϕ_1=3, ϕ_2=1, Re=150, A=0.6, St=0.01), (m) (ϕ_1=3, ϕ_2=1, Re=150, A=0.6, St=0.05), (n) (ϕ_1=3, ϕ_2=1, Re=150, A=0.6, St=0.1), (o) (ϕ_1=3, ϕ_2=1, Re=150, A=0.6, St=0.25), (p) (ϕ_1=3, ϕ_2=1, Re=150, A=0.6, St=0.5), (r) (ϕ_1=3, ϕ_2=1, Re=150, A=0.6, St=2.5), (s) (ϕ_1=3, ϕ_2=1, Re=150, A=0.6, St=5)

4. Conclusions

By forming the channel through with the fluid passes as a step form, it is seen that the flow is directly oriented, and some changes occur in the step zone and the lower surface of the channel. When the changes in velocity for different Re are examined, it is seen that the circulation at the step increases as the Re increases for five different conditions including water and nanofluids containing different volume ratios of Al_2O_3 (1-5%) and different volume ratios of Cu (1% or 2%).

When the changes in temperature for different Re are examined, it is seen that the downstream temperature increases as the Re increases for five different conditions including water and nanofluids containing in the main fluid and in all nanofluids, the increase in the Re enhances the heat transfer capability.

It is seen that the heat transfer capabilities of the nanofluids are better than water. It is also seen that the heat transfer capabilities of the nanofluids increase as the volume ratios of the nanoparticles they contain increase. A significant increase in the heat transfer capability of the nanofluid is observed as the volume ratio of Cu nanoparticle increases.

It is determined that the friction coefficient decreases with the increment in Re. Since the velocity increases with increment in Re, in this situation, the friction coefficient decreases. It is seen that the friction coefficient increases as the Strouhal number increases. This situation is caused by the increase in frequency values directly proportional to the increase in the Strouhal number.

The increase in Re increases the heat transfer capability in water, which is the main fluid, and the nanofluids under pulsating flow condition. It is seen that the increase in the velocity amplitudes of water and nanofluids causes significant increases in the Nu. It is understood from these figures that velocity amplitude value in pulsating flow has a great significance in heat transfer capability.

Nomenclature

k	Thermal conductivity coefficient (W/mK)
f	characteristic frequency
μ	dynamic viscosity (kg/ms)
g	gravitational force (m/s2)
Re	Reynolds number (ρvD/μ)
Eu	Euler number
Nu	Nusselt number (hD/k)
α	thermal diffusion coefficient
Φ_1	Volume fraction of Al_2O_3 nanoparticle
Φ_2	Volume fraction of Cu nanoparticle
τ	shear stress (Pa)
h	convection heat transfer coefficient (W/m^2K)
T	temperature (K)
θ, r	cylindrical coordinates
ρ	density of fluid (kg/m^3)
ν	kinematic viscosity (m^2/s)
P	pressure (Pa)
St	Strouhal number (fL/U)
Fr	Froude number
C_p	specific heat (J/kgK)
C_f	friction coefficient
u, v, w	velocity (m/s)
BFS	backward-facing step flow
L	characteristic length

Subscripts

f	fluid
nf	nanofluid
s	nanoparticle

References

Abu-Mulaweh H.I., Armaly B.F., Chen T.S., (1995), Laminar natural convection flow over a vertical backward-facing step, *Journal of Heat Transfer*, **117**, 895-901.

Abu-Nada E., (2008), Application of nanofluids for heat transfer enhancement of separated flows encountered in a backward-facing step, *International Journal of Heat and Fluid Flow*, **29**, 242-249.

Al-Aswadi A.A., Mohammed H.A., Shuaib N.H., Campo A., (2010), Laminar forced convection flow over a backward facing step using nanofluids, *International Communications in Heat and Mass Transfer*, **37**, 950-957.

Atabek H.B., Chang C.C., (1961), Oscillatory flow near the entry of circular tube, *Journal of Applied Mathematics and Physics (ZAMP)*, **12**, 185-201.

Baek B.J., Armaly B.F., Chen T.S., (1993), Measurements in buoyancy-assisting separated flow behind a vertical backward-facing step, *Journal of Heat Transfer*, **2**, 403-408.

Chiang T.P Sheu, (1999), TWH. A numerical revisit of backward-facing step flow problem, *Physics of Fluids*, **11**, 862-874.

Duca G., Covaliov V., Covaliova O., (2020), Production, structure and photocatalytic properties of nanotubular TiO_2, *Environmental Engineering and Management Journal*, **18**, 65-74.

Gerrard J.H., Hughes M.D., (1971), The flow due to a pulsating piston in a cylindrical tube a comparison between experiment and a simple inlet flow theory, *Journal of Fluid Mechanics*, **50**, 97-106.

Hamilton R.L., Crosser O.K., (1962), Thermal conductivity of heterogeneous two- component systems, *I & EC Fundamentals*, **1**, 182-191.

Hino M., Savamato M., Takasu S., (1976), Experiments on transition to turbulence in an oscillatory pipe flow, *Journal of Fluid Mechanics*, **75**, 193-207.

Honami S., Nakajo I., (1986), A reattaching shear layer to the curved surfaces over a backward-facing step, *The American Society of Mechanical Engineers (ASME)*, 86-WA/FE-9.

Hong B., Armaly B.F., Chen T.S, (1993), Laminar mixed convection in a duct with a backward-facing step – the effects of inclination angle and Prandtl number, *International Journal of Heat and Mass Transfer*, **36**, 3059-3067.

Hwang K.S., Jang S.P., Choi S.U.S., (2009), Flow and convective heat transfer characteristics of water-based Al2O3 nanofluids in fully developed laminar flow regime, *International Journal of Heat and Mass Transfer*, **52**, 193-199.

Khanafer K., Al-Azmi B., Al-Shammari A., Pop I., (2008), Mixed convection analysis of laminar pulsating flow and heat transfer over a backward-facing step,

International Journal of Heat and Mass Transfer, **52**, 5785-5793.

Lin J., Armaly B., Chen T., (1990), Mixed convection in buoyancy-assisted vertical backward-facing step flows, *International Journal of Heat and Mass Transfer*, **33**, 2121-32.

Mansour R.B., Galanis N., Nguyen C.T., (2011), Experimental study of mixed convection with water-Al2O3 nanofluid in inclined tube with uniform wall heat flux, *International Journal of Thermal Sciences*, **50**, 403-410.

Maxwell J.C., (1873), *Electricity and Magnetism*, Clarendon Press, Oxford, UK.

Maxwell-Garnett J.C., (1904), *Colours in Metal Glasses and in Metallic Films*, Philosophical Transactions the Royal SocietyA, **203**, 385-420.

Mehrez Z., Cafsi A.E., (2019), Forced convection magnetohydrodynamic Al_2O_3–Cu/water hybrid nanofluid flow over a backward-facing step, *Journal of Thermal Analysis and Calorimetry*, **135**, 1417-1427.

Mehrez Z., Bouterra M., Cafsi A.E., Belghith A., Quéré P.L., (2010), Simulation of the periodically perturbed separated and reattaching flow over a backward-facing step, *Journal of Applied Fluid Mechanics*, **3**, 1-8.

Zamzari F., Mehrez Z., Cafsi A.E., (2019), Heat Transfer Enhancement of Pulsating Flow in an Open Cavity Subjected to Uniform Magnetic Field, *Fluid Dynamics*, **54**, 428-438.

Mehrez Z., Cafsi A.E., (2017), Thermodynamic analysis of Al2O3–Water nanofluid flow in an open cavity under pulsating inlet condition, *International Journal of Applied and Computational Mathematics*, **3**, 489-510.

Moukalled F., Doughan A., Acharya S., (2000), Parametric study of mixed convection in channels with concave and convex surfaces, *International Journal of Heat and Mass Transfer*, **43**, 1947-1963.

Murshed S.M.S., Leong K.C., Yang C., (2008), Investigations of thermal conductivity and viscosity of nanofluids, *International Journal of Thermal Sciences*, **47**, 560-568.

Murshed S.M.S., Leong K.C., Yang C., (2009), A combined model for the effective thermal conductivity of nanofluids, *Applied Thermal Engineering*, **29**, 2477-2483.

Naphon P., Sriromruln P., (2006), Single-phase heat transfer and pressure drop in the micro-fin tubes with coiled wire insert, *International Communications in Heat and Mass Transfer*, **33**, 176-183.

Naphon P., Wongwises S., Wiriyasart S., (2013), Application of two-phase vapor chamber technique for hard disk drive cooling of PCs, *International Communications in Heat and Mass Transfer*, **40**, 32-35.

Naphon P., Kornkumjayrit K., (2008), Numerical analysis on the fluid flow and heat transfer in the channel with V-shaped wavy lower plate, *International Communications in Heat and Mass Transfer*, **35**, 839-843.

Naphon P., Sookkasem A., (2007), Investigation on heat transfer characteristics of tapered cylinder pin fin heat sinks, *Energy Conversion and Management*, **48**, 2671-2679.

Naphon P., Wiriyasart S., (2018a), Pulsating flow and magnetic field effects on the convective heat transfer of TiO_2-water nanofluids in helically corrugated tube, *International Journal of Heat and Mass Transfe*r, **125**, 1054-1060.

Naphon P., Wiriyasart S., (2018b), Experimental study on laminar pulsating flow and heat transfer of nanofluids in micro-fins tube with magnetic fields, *International Journal of Heat and Mass Transfer*, **118**, 297-303.

Naphon P., Wiriyasart S., (2017), Pulsating TiO_2/water nanofluids flow and heat transfer in the spirally coiled tubes with different magnetic field directions, *International Journal of Heat and Mass Transfer*, **115**, 537-543.

Naphon P., Wiriyasart S., Arisariyawong T., Nualboonrueng T., (2017), Magnetic field effect on the nanofluids convective heat transfer and pressure drop in the spirally coiled tubes, *International Journal of Heat and Mass Transfer*, **110**, 739-745.

Naphon P., Wiriyasart S., Arisariyawong T., (2018), Artificial neural network analysis the pulsating Nusselt number and friction factor of TiO2/water nanofluids in the spirally coiled tube with magnetic field, *International Journal of Heat and Mass Transfer*, **118**, 1152-1159.

Naphon P., (2016), Experimental investigation the nanofluids heat transfer characteristics in horizontal spirally coiled tubes, *International Journal of Heat and Mass Transfer*, **93**, 293-300.

Nekoeinia M., Khodadeh-Tehrani A., Moradlou O., Semnani A., Kolahdoozan M., Kazemi H., Dehkordi M.K., (2020), Fast removal of malachite green from aqueous solutions using highly hydrophobic water–dispersible magnetic nanocomposite, *Environmental Engineering and Management Journal*, **18**, 1079-1096.

Peacock J.A., Stairmand J.W., (1983), Film gauge calibration in oscillatory pipe flow, *Journal of Physics e Scientific Instruments*, **16**, 571-576.

Selimefendigil F., Öztop H.F., (2013), Numerical analysis of laminar pulsating flow at backward-facing step with an upper wall mounted adiabatic thin fin, *Computers and Fluids*, **88**, 93-107.

Terhaar S., Velazquez A., Arias J.R., Sanchez-Sanz M., (2010), Experimental study on the unsteady laminar heat transfer downstream of a backwards facing step, *International Communications in Heat and Mass Transfer*, **37**, 457-462.

Valipour A., Abbasitabar F., Zare-Shahabadi V., (2020), Zinc hydroxide nanoparticles-modified clay for ultrasound-assisted removal of methylene blue, *Environmental Engineering and Management Journal*, **18**, 453-466.

Vogel J.C., Eaton J.K., (1985), Combined heat transfer and fluid dynamic measurements downstream of a backward-facing step, *Journal of Heat Transfer*, **83**, 922-929.

Wang X., Mujumdar A.S., (2007), Heat transfer characteristics of nanofluids a review, *International Journal of Thermal Sciences*, **46**, 1-19.

Wang B.X., Zhou L.P., Peng X.F., (2003), A fractal model for predicting the effective thermal conductivity of liquid with suspension of nanoparticles, *International Journal of Heat and Mass Transfer*, **46**, 2665-2672.

Williams P.T., Baker A.J., (1997), Numerical simulations of laminar flow over a 3d backward-facing step, *International Journal for Numerical Methods in Fluids*, **24**, 1159-1183.

Xuan Y., Li Q., (2000), Heat transfer enhancement of nanofluids, *International Journal of Heat and Fluid Flow*, **21**, 58-64.

Zhao T.S., Cheng P., (1998), *Heat Transfer in Oscillatory Flow, Annual Review of Heat Transfer*, vol.IX, , The Hong Kong University of Science&Technology, Clear Water Bay, Kowloon, Hong Kong.